Photo atalyti adi al Al ylation of le tro hili lefins by en yli and Al yli in ulfinates

Is anthropogenic land-subsidence a possible driver of riverine flood-hazard dynamics? A case study in Ravenna, Italy

F. Carisi[1]*, A. Domeneghetti[1], M. G. Gaeta[2], A. Castellarin[1]

[1] *DICAM – School of Civil, Chemical, Environmental and Materials Engineering, University of Bologna, Bologna, Italy*
francesca.carisi@unibo.it

[2] *CIRI – EC, Fluid Dynamics Unit, University of Bologna, Italy*

Abstract:

We investigate possible changes in flood-hazard over a 77-km^2 area around the city of Ravenna. The subsidence rate in the area, naturally a few mm year^{-1}, increased dramatically after World War II because of groundwater and natural gas extraction, exceeding 110 mm year^{-1} and resulting in cumulative drops larger than 1.5 m. The Montone-Ronco river system flows in the southern portion of the area, which is protected against frequent flooding by levees. We performed two-dimensional simulations of inundation events associated with levee breaching by considering four different terrain configurations: current topography and a reconstruction of ground elevations before anthropogenic land-subsidence, both neglecting and representing main linear infrastructures (e.g. roads, artificial channels, etc.). Results show that flood-hazard changes due to anthropogenic land-subsidence (e.g. significant changes in computed water depth and velocity) are observed over less than 10% of study area and are definitely less important than those resulting from the linear infrastructures construction.

Key words anthropogenic flood-hazard alterations; inundation modelling; role of linear infrastructures; TELEMAC-2D; Flood Area Index FAI; levee-breaching.

1 INTRODUCTION

Between 2006 and 2015, flooding has been the third major cause of economic losses worldwide among all natural hazards (the firsts being earthquakes and storms), resulting in a total damage in excess of US $300 billion, and the first in terms of overall number of affected people (i.e. more than 0.8 billion people). During the same decade, flooding is ranked first in terms of both total damage (i.e. ~ US $51 billion) and number of affected people (i.e. ~ 4 million people) in Europe (D. Guha-Sapir *et al.*). According to these figures, flooding severely impacts humans and their economies (i.e. ~ US $30 billion and ~80 million people per year, globally) and this is not surprising as, for example, nine of the ten largest urban agglomerates worldwide are located in flood-prone areas (Di Baldassarre *et al.* 2013).

Further analyses of the CRED/OFDA Database reveal that during the three decades 1986-1995, 1996-2005 and 2006-2015 flooding affected a stable number of people worldwide (0.8-1.0 billion people), whereas the total damage increased dramatically (i.e. ~100% per each decade). Correctly interpreting the dynamics of flood-risk (defined herein as the product of hazard and damage) and identifying its major drivers are therefore of paramount importance (see e.g. Ciullo *et al.* 2017). The scientific literature seems to show a consensus on the most influential drivers of flood-risk dynamics, identifying them in climate variability and human pressure. Focusing on the role and impact of anthropization occurred during the last century, several studies show that flood-risk changes mainly result from land-use and land-cover modifications increasing exposure to flooding, rather than climate variability and change (see e.g. Bouwer *et al.* 2010, Di Baldassarre *et al.* 2013). Domeneghetti *et al.* (2015) investigate trends on long historical flood sequences observed for the Po River and demographic as well as land-use changes occurred in the last five decades and show that major fluctuations in flood-risk are associated with anthropization and urban sprawl within Po River floodplains, confirming previous analyses on the same study area (see e.g. Zanchettini *et al.* 2008, Montanari *et al.* 2013). These studies share the main background idea of Panta-Rhei "Change in hydrology and society - Everything Flows", the scientific decade 2013–2022 of IAHS dedicated to research activities on change in hydrology and society, emphasizing the importance of considering people and water systems as two closely related components (see Sivapalan *et al.* 2012, Koutsoyiannis 2013, Montanari *et al.* 2013).

Recent literature is addressing the understanding and representation of complex interactions between society and flood hydrology and clearly shows that these are particularly intense in floodplains around the world where residential, industrial and agricultural areas, infrastructures, flood control measures and river engineering have gradually co-evolved during centuries (see e.g. Castellarin *et al.* 2011, Ciullo *et al.* 2017).

Among all human activities that can impact flood-hazard (and hence flood-risk) dynamics in floodplains and flood-prone areas, our study focuses on the human-induced land-subsidence in densely populated areas, i.e. the accelerated ground-lowering due to the pumping of underground fluids. Potok (1991) pointed out evidences of land-surface subsidence due to the withdrawal of oil and gas in the Baytown, Texas, already in 1918, but this phenomenon, which nowadays is well-known, was observed in different parts of the world, mainly during the second half of the 20th century. Literature reports several examples of severe human-induced

ground-lowering in Mexico (see e.g. Ortega-Guerrero *et al.* 1999), Japan (see e.g. Daito and Galloway 2015; Gotoh *et al.* 2009), Thailand (see e.g. Phien-wej *et al.* 2006), Bangladesh (see e.g. Brown and Nicholls 2015; Howladar and Hasan 2014) and Philippines (see e.g. Rodolfo and Siringan 2006), which caused problems to building foundations and to sewer and transportation systems, as well as the accumulation of storm water during the rainy season, sometimes resulting in extensive flooding of farmland.

The flooding problems induced by land-subsidence in coastal areas have been deeply investigated and understood. Yin *et al.* (2013) reported the decrease of the return period of coastal flooding due to the combined impact of eustatic sea-level rise and land subsidence. Schmidt (2015) and references therein highlight an alarmingly increase in the frequency of flood events in deltas during the last decades due to the human-induced soil compaction and a reduced deposition of sediments on floodplains, the latter associated with the construction of levee systems. Together with the rising sea level, these phenomena cause a growth of the water level in coastal areas, potentially increasing coastal or tidal flooding in low-lying areas that were previously above high-tide level (Marfai and King 2008).

Literature on possible alterations induced by anthropogenic land-subsidence on riverine flood hazard and risk in flood-prone areas, instead, is still sparse; yet the problem is worth investigating as, during the last decades, there has been a remarkable growth of urbanization in dyke-protected floodplains of major Italian (and European) rivers. In fact, the presence of levee systems encourages the development of residential areas and industrial/agricultural activities in areas that are close to waterbodies (see e.g. . Castellarin *et al.* 2011b, Di Baldassarre *et al.* 2009a, Domeneghetti *et al.* 2015). In addition, it is worth noting that many existing embankment systems were built centuries ago; they prevented the riverbed to gradually adapt to changes of topography induced by natural (and anthropogenic) land-subsidence, and this may have resulted in significant modifications of the spatial distribution of flood hazard in case of embankment failure.

Our study aims at better understanding whether and to what extent human-induced, or human-accelerated, ground-lowering can alter flood hazard associated with riverine inundations. To this aim, we focused on the area near the city of Ravenna (northern Italy), one of the Italian most prominent cases of anthropogenic land-subsidence. The ground-lowering of the study area, which accelerated after World War II due to intense groundwater and natural gas extraction, reached peaks of more than 1.5 m in nearly 100 years close to the historical city centre (Gambolati *et al.* 1991, Carminati and Martinelli 2002). In order to quantify the potential influence of land-subsidence on the flood-hazard dynamics and to compare it with the influence of other anthropogenic drivers, we simulated several inundation scenarios resulting from possible levee failures in the proximity of the city of Ravenna through a fully bi-dimensional (2D) model. We implemented the 2D model considering current and past (i.e. reconstruction of 1897 ground elevation) topographies, as well as presence or absence of the main linear infrastructures (e.g. road and railway embankments and land-reclamation channels).

The area around the city of Ravenna and the city itself have undergone major changes after 1897 in terms of land-use, built-up areas, civil infrastructures, flood mitigation measures, etc. It is worth noting here that the main goal of our study is not to reproduce faithfully and in every possible detail the flood hazard

conditions in 1897 and nowadays. Rather differently, we take advantage of the noteworthy case study of Ravenna aiming at assessing the potential impacts on riverine flood hazard of anthropogenic land-subsidence on its own; for this reason, our scenarios deliberately hold all other possible (anthropogenic and natural) drivers of flood hazard and risk dynamics constant. The comparison of scenarios is therefore targeted at clearly showing possible alterations of flood hazard associated with land-subsidence, avoiding masking effects associated with changes of some other overlapping drivers. The specific focus on linear infrastructures (i.e. channels and embankments) highlighted above goes along the same lines; since anthropogenic land-subsidence alters the floodplain morphology, we assess its impact on flooding potential relative to other anthropogenic topographical features that may or may not be correctly reproduced in the modelling exercises, depending e.g. on the resolution of the available DEMs and modellers' choices. Ultimately, our study addresses the following research questions:

1) can anthropogenic land-subsidence alter riverine flood hazard in a given flood-prone area?
2) can it significantly modify the inundation intensity (e.g. extent and spatial distribution of flooded areas; spatial distribution of hydrodynamic variables such as water depth, h, current velocity, v and/or intensity, $h \cdot v$)?
3) are its effects more intense than those resulting from other anthropogenic alterations of floodplain morphology, such as construction of roads, railways and artificial channels?

2 STUDY AREA

The study area consists of the 77-km^2 area around the city of Ravenna, in the Emilia-Romagna region of Italy, about 60 km south of the Po River delta - see Fig. 1(a). With a municipal area of 653 km^2 and a population of 160 000 inhabitants, the city boasts a long and rich cultural history: historians set its foundation in the eighth century B.C., making it one of the oldest Italian towns. During the three centuries after 400 A.D., Ravenna became a capital three times: of the Western Roman Empire, of Theodoric King of the Goths and of the Byzantine Empire in Europe. Furthermore, after the invasion of the Lombards in 751, it was chosen as the seat of their kingdom. The magnificence of this period has left Ravenna with a great heritage of historical buildings: eight UNESCO World Heritage Sites are located in the city (source: UNESCO).

The study area is a densely urbanized and commercial district, which is characterized by high population density (240 inhabitants/km^2, census by Istat – Italian National Institute of Statistics), as well as a complex network of human infrastructures - see Fig. 1(b). Although Ravenna is nowadays an inland city, it is still connected by the Candiano Canal to the Adriatic Sea, which is located a few kilometres east of the city - see Fig. 1(c). The Montone River and the merger of Montone and the Ronco Rivers (i.e. Fiumi Uniti River) flow through the city - see Fig. 1(c), which is entirely protected against frequent flooding by a system of artificial embankments.

Like many other coastal lowlands and deltaic plains, the eastern Po plain and, in particular, the area where Ravenna is located, lies on a subsiding sedimentary basin that experienced over centuries extremely significant changes in terms of ground elevation. The local rate of land-subsidence is naturally in the order of a few mm per year, but it increased enormously after World War II, as shown, for example, in the ground elevation analysis by Bitelli *et al.* (2000), most likely due to an increase in the extraction of deep non-renewable groundwater associated with the economic growth and industrial expansion of the area. Gambolati *et al.* (1991) show how this and the subsequent exploitation of several on-shore and off-shore deep gas reservoirs in the Ravenna area increased the rate of land-subsidence up to some centimetres per year. The close relationship between groundwater pumping and land-subsidence is confirmed by numerous studies. Carminati and Martinelli (2002) show the link between the lowering of subsidence rate in recent years and the application of a national government law that enforced an important decrease of groundwater withdrawal. Teatini *et al.* (2005) affirm that during the late 1970s and 1980s the construction of new public aqueducts exploiting surface water has significantly reduced the subsurface water consumption and consequently the settlement rates reverted to the pre-war values. Teatini *et al.* (2005) also constructed a detailed georeferenced map of land-subsidence in the eastern Po River plain over the period 1897-2002, based on the main levelling surveys available in the last century (Military Geographic Institute - IGM, Ravenna Reclamation Authority, Geological Service of the Ravenna Municipality, Regional Agency for Environmental Protection - ARPA and National Hydrocarbons Authority – Exploration and Production - ENI-E&P).

Cumulative land-subsidence evaluated by Teatini *et al.* (2005) is illustrated in Fig. 1(c), which shows drops larger than 1 m over more than one third of the area, with peaks beyond 1.5 m over a 10-km^2 area located between the historical centre and the Adriatic coast. The ground-lowering patterns are particularly striking also in terms of subsidence gradients, which can be as high as 0.3 m km^{-1}, being therefore comparable with riverbed slopes of natural streams flowing in the area (e.g. bed slope of Montone-Ronco river system is approximately 0.7 m km^{-1}).

3 TOPOGRAPHY OF THE STUDY AREA

3.1 Current and past terrain elevations

The study-area current topography is described through a contemporary 5m horizontal resolution Digital Elevation Model (DEM), made available as a GIS Service by the cartographic office of the Emilia-Romagna Region - see Fig. 2(a). The cumulative land drop observed up to 2002 and reported in Teatini *et al.* (2005) were summed to the current 5m DEM, therefore obtaining another 5m DEM that describes the ground elevation in 1897. We neglected changes in ground elevations between 2002 and today, which have been minimal. According to Fig. 1, the backward-warping process increased the ground elevations the most in the North-eastern portion of the study area (ca. 155 cm), and the least in the South-western area, located approximately 4 km from the city of Ravenna (ca. 80 cm).

3.2 Main infrastructures

Even though the main focus of our study regards anthropogenic land-subsidence, human presence and activity on floodplains lead to other kinds of topography alterations that are potential drivers of flood hazard dynamics (e.g. construction of main road infrastructures, complex artificial drainage and land-reclamation networks, systems of secondary dikes, etc., see Domeneghetti 2014, Dottori *et al.* 2013, Heilemariam *et al.* 2013). Possible changes in flooding intensity and flood-hazard associated with land-subsidence and their significance need to be compared to changes that result from other anthropogenic alterations of the topography. Among these, we considered the main road and rail infrastructures and land-reclamation channels existing in the study area - see Fig. 2(a).

The DEM resolution (i.e. 5 m) cannot grasp the details of these existing discontinuities, apart from some of the larger ones; main railways and land-reclamation channels could therefore be mis-represented and discontinuous due to the topology of the DEM grid. For this reason, two additional DEMs were created, one from the current DEM and the other from the backward-deformed DEM, in which major topographic discontinuities have been manually incorporated according to field surveys, digital databases and photos (sources: Google Street View; digital cartographic database of the Emilia-Romagna Region). In particular, continuous 1m-tall railway embankments were included in the topography and continuous 1.5m-deep land reclamation channels were carved to match the existing layout of main linear infrastructures - see Fig. 2(a).

3.3 Considered terrain configurations

Our study investigates the flooding intensity in four different terrain configurations, obtained by combing two different topographies (past and present, related to land-subsidence) with the presence or absence of continuous linear infrastructures:

- Current: current morphology, as represented by the contemporary 5m DEM;
- Current and Infrastructures: current morphology with continuous infrastructures;
- Past: 1897 topography obtained by backward-deforming current morphology on the basis of cumulative land-subsidence illustrated in Teatini *et al.* (2005);
- Past and Infrastructures: 1897 topography obtained by backward-deforming Current and Infrastructures on the basis of cumulative land-subsidence illustrated in Teatini *et al.* (2005).

4 HYDRODYNAMIC MODELLING

4.1 Numerical models

Inundation intensity and flood-hazard for the four considered terrain configurations were studied using a modelling cascade, that includes a one-dimensional (1D) model of the Montone-Ronco river system and a fully two-dimensional (2D) model simulating the inundation dynamics in the flood-prone area. In particular, the hydraulic behaviour of the Montone-Ronco river system is reproduced by using the 1D HEC-RAS model (US Army Corps of Engineers, Institute for Water Resources, Hydrologic Engineering Center 2010), which solves the De Saint Venant equations for unsteady open-channel flow through the UNET code (Barkau 1997). The fully-2D model adopted for the floodplain flow is the TELEMAC-2D model, which solves the 2D shallow water (or depth averaged) De Saint Venant equations (Galland *et al.* 1991, Hervouet and Van Haren 1996), largely validated in hydraulics (see e.g. Fernandes *et al.*, 2001) and coastal engineering (see e.g. Gaeta *et al.*, 2016). It can represent complex floodplain topographies and both wetting and drying dynamics (Horritt *et al.* 2007). One of the main advantages of TELEMAC-2D is the use of non-structured computational meshes that can accurately and effectively describe topographic discontinuities that affect the inundation process (e.g. levees, road and railway embankments and channels; see e.g. Brath and Di Baldassarre 2006, Domemeghetti 2014, Di Baldassarre *et al.* 2009a and 2009b).

The HEC-RAS model is used in our study for simulating the hydraulic behaviour of the Montone-Ronco river system and the discharge outflowing hypothetical levee breaches, which in turn is used as inflow boundary condition for reproducing the inundation dynamics with TELEMAC-2D.

4.2 Implementation of the hydrodynamic numerical models

We implemented a numerical 1D hydraulic model of the middle-lower portion of Montone-Ronco river system - nearly 28 km in total, to the mouth of the Fiumi Uniti River into the Adriatic Sea, see Fig. 2(a). River geometry was modelled on the basis of 85 cross-sections retrieved from the regional river basins authority (AdB-RR). Our numerical simulations identified in nearly 550 $m^3 s^{-1}$ the design discharge of the lowest part of the Montone River, higher discharge values result in overtopping of existing levee system (see e.g. the report form the local river basin authority, AdB-RR 2011). Therefore, this study refers to a synthetic hydrograph with a flow peak of 550 $m^3 s^{-1}$ and a wave shape obtained by re-scaling a historical event observed at Ponte Vico streamgauge (located immediately upstream the considered river stretch). In addition, we adopted as downstream boundary condition a constant water surface elevation at river's outlet into the Adriatic Sea. We deemed these simplifications to be an acceptable working hypothesis; as stated in the introduction, our study aims at comparing flooding intensity resulting from realistic flood events over different terrain configurations rather than performing a detailed reconstruction of historical flood events.

We hypothesized four different levee-breaching scenarios along the left Montone-Ronco embankment - Fig. 2(a) reports numbers to identify the breaches' locations. For each one of them, we modelled an instantaneous breach formation concurrently with the transit of the flood wave peak, a breach width of 120 m

and a full vertical breaching (from the levee crest to ground elevation). The breach width has been set according to sizes of historical breaches observed in similar Italian rivers (e.g. Serchio levee failure in December 2009, Secchia levee failure in January 2014 and others; see Orlandini *et al.* 2015, Govi and Turitto 2000, catalogue of historical levee breaches along the Po River).

We focused on the embankment stretch close to the city of Ravenna, following the indications of the local river basin authority, which identifies that particular stretch as the most exposed one to overtopping and stability issues (see Reno, Romagna and Marecchia-Conca rivers basins authorities - AdB-Reno, AdB-RR, and AdB-Marecchia-Conca 2016). We modelled four different breaching events - see red triangles numbered from 1 to 4 in Fig. 2(a), overall stretch length: 6 km - for each terrain configuration identified in Paragraph 3.3. The main reasons are two. First, due to the morphology of the system (river and left-levee crest), the probability of levee overtopping is homogeneous along the 6-km stretch between points 1 and 4 - Fig. 2(a); hence it is impossible to identify the most likely breaching location *a-priori*. Second, we wanted the results of our study to be independent of the breaching location and therefore we considered four uniformly distributed breaching locations that are located both upstream and downstream two large embankments which can greatly affect the flooding dynamics in the flood-prone area - see Fig. 2(a): the first is the embankment of a large state-road, which is accurately captured by the available 5m DEM; the second is the railroad embankment that has been manually represented in the terrain configurations that consider main linear infrastructures (i.e. Current and Infrastructures and Past and Infrastructures).

HEC-RAS simulations of the four breaching events showed very limited differences in terms of peak-flow and overall volume of the simulated outflowing hydrographs. Therefore, for the sake of consistency and comparability of results, we referred to the mean outflowing hydrograph for all inundation scenarios. The mean simulated outflowing discharge (with an overall flood volume equal to $3 \cdot 10^6$ m^3) was adopted as liquid boundary condition for the TELEMAC-2D simulations focusing on the inundation intensity in the 77-km^2 study area.

We constructed a non-structured computational mesh used for all the performed 2D simulations - see Fig. 2(b); the mesh consists of 133,722 triangular elements and 67,284 nodes and provides an accurate representation of natural complexities as well as linear infrastructures, when present - the element size varies from 350 to 0.5 m, moving from flatter zones to major discontinuities, see Fig. 2(b). The elevation of each node in the mesh was then retrieved from the 5m DEMs used to create the four terrain configurations (see Paragraph 3.3): Current, Current and Infrastructures, Past, Past and Infrastructures. Floodplain Manning's roughness coefficient (n) was assigned according to indications reported in the literature (see e.g. Chow 1959, Vorogushyn 2008, Domeneghetti *et al.* 2013) as a function of land-use characteristics retrieved from CORINE (COoRdinated INformation on the Environment) 2012 dataset (EEA 2016): we adopted $n = 0.2$ $m^{-1/3}s$ for urban and industrial areas and 0.035 $m^{-1/3}s$ for agricultural ones.

The lack of inundation data did not enable us to validate the 2D hydrodynamic model, nevertheless the same numerical model has been applied in other case studies in Emilia-Romagna providing realistic representations of the observed inundation intensity (Di Baldassarre *et al.*, 2009b); furthermore, we performed

a sensitivity analysis of the study results, assessing the potential impact of alternative roughness coefficients. The sensitivity analysis is described in detail in Section 5.4, which closes the presentation and discussion of results. As already mentioned, the different scenarios considered in this study neglect changes in all other potential natural and anthropogenic drivers of flood risk dynamics (e.g. historical land-use changes, levee adjustments over time, increase of the built up area, etc.). These working hypotheses enable us to directly compare the flooding scenarios with each other and to better understand the impacts of anthropogenic land-subsidence on flood-hazard dynamics. For the same reason, infrastructures and levees elevations have been modified only in accordance with the ground-lowering rate indicated by Teatini *et al.* (2005), without considering other modifications due to adjustments that the structures have suffered over the decades.

5 RESULTS AND DISCUSSION

We present the results of our analysis focusing on the most representative hydraulic indices obtained from all simulations, namely:

- computed flooded area;
- maximum computed local water depth, h (m);
- maximum computed local water velocity, v (m s^{-1});
- maximum computed local current intensity, $i = h \cdot v$ (m^2 s^{-1}).

For the sake of clarity, we organized the presentation and discussion of results by addressing the three research questions we set in the introduction.

5.1 Can anthropogenic land-subsidence alter riverine flood hazard?

Figure 3 illustrates the flooded areas resulting from a given inundation event and two different terrain configurations. In this context, we defined as flooded area the floodplain portion for which the computed maximum water depth that results from the model simulations exceeds 0.1 m. Figure 3 shows the comparison between flooded areas for Current and Past terrain configurations under the same levee breaching - breach location no. 2 in Fig. 2(a). Light-grey areas in Fig. 3 are flooded in both Current and Past configurations; dark-grey areas are flooded in Past configuration only, while black areas are flooded in Current configuration only. The most striking feature of Fig. 3 is certainly the fact that the majority of inundated areas is flooded in both terrain configurations. Nevertheless, it is worth noting that the current terrain configuration (Current) is associated with larger inundated areas near the city of Ravenna (black area), where more damages are expected in terms of residential areas and industrial activities. Areas flooded only for Past terrain configuration, instead, are mainly located in rural zones in the Eastern portion of the study area (dark-grey areas).

Concerning Current and Past terrain configurations, we obtained similar results by simulating the inundation scenarios resulting from the three remaining breaching events; additional simulations are not

illustrated herein for the sake of brevity. Based on these outcomes, we can state that anthropogenic land-subsidence may have affected the inundation hazard in the study area, but the significance of these flood-hazard alterations appears to be limited, at least in terms of floodable areas.

5.2 Can anthropogenic land-subsidence significantly modify the flooding intensity?

The literature clearly indicates that tangible damages and economic losses caused by inundation events are associated with water depth, together with other hydraulic variables or indices (e.g. water velocity, see e.g. Green *et al.* 2011, Meyer *et al.* 2013, Merz *et al.* 2013), and damages typically occur when at least one of these indices becomes significant. Significance in this context is identified empirically and is expressed in terms of threshold values. According to Kreibich *et al.* (2009), we adopted three definitions of significantly flooded area (i.e., flooding that produces more than slight structural damages and more than moderate non-structural damages when goods and assets are at risk), focusing in turn on one of the three different hydraulic indices:

(i) maximum local water depth (h) higher than 50 cm;

(ii) maximum local water velocity (v) higher than 0.25 m s^{-1};

(iii) maximum local current intensity (i) higher than 0.1 m^2 s^{-1}.

Therefore, considering one hydraulic index at a time (i.e. either h, v, or i), we compared the extent of significantly flooded areas associated with all four terrain configurations (i.e., Past, Current, Past and Infrastructures, Current and Infrastructures) by means of an adaptation of the Flood Area Index (FAI, see Schumann *et al.* 2009, Falter *et al.* 2013). In particular, for one breach event, we compared pairs of terrain configurations (e.g. Current and Past and Infrastructures) by means of:

$$\mathrm{FAI} = \frac{A}{A+B+C} \qquad (1)$$

where:

A is the extent of the area that is significantly flooded for both configurations;

B is the extent of the area, that results significantly flooded in one of the two configurations only;

C is the opposite of B, i.e. the area significantly flooded in the other configuration only.

Areas A, B and C are those in which one hydraulic index (either h, v, or i) satisfies the condition given above (i.e. either (i), (ii), or (iii)). The closer to 1.0 the FAI coefficient, the higher the similarity between the significantly flooded areas in the two terrain configurations.

Table 1 shows FAI values for the three hydraulic indices considered in the study, indicating the pairs of terrain configurations being considered. Specifically, once defined the terrain configurations that are compared, the value reported in Table 1 represents the average FAI value obtained from the comparison of all the inundations resulting from the four levee breaches - see Fig. 2(a). In particular, aiming at addressing the research question of the present section, we should focus on the first two rows of Table 1. These compare current and past terrain configurations in a consistent way as far as the presence of linear infrastructures is concerned, meaning that main linear infrastructures are either present or neglected in both terrain

configurations. The FAI values reported in the first two rows of Table 1 indicates that there are differences between the results obtained for compared terrain configurations, that is anthropogenic land-subsidence does alter the extent of significantly flooded areas. Yet, the modifications appear to be limited, being the FAI value always above 0.75 (i.e. differences are relative to less than 25% of the significantly flooded area), and close to 0.9 (differences are in the order of 10% of the flooded areas) when we define significantly flooded areas by looking at water depth only. Are these differences comparable with the alterations in flooding potential that result from the construction of linear infrastructures? We address this problem in the next paragraph.

5.3 Are the effects of anthropogenic land-subsidence more intense than those resulting from linear infrastructures?

Similarly to Fig. 3, Fig. 4 shows an example highlighting the differences in terms of flooded area simulated for two terrain configurations and a given levee-breaching scenario. In this case, we refer to the current topography and the two terrain configurations differ only in terms of main linear infrastructures (i.e., railways, roads and land-reclamation channels), which are either neglected, or correctly reproduced (i.e. Current or Current and Infrastructures configurations, respectively).

Figure 4 clearly shows that the presence of linear infrastructures strongly affects the flooding extent. The common flooded area in both the configurations (light-grey colour) represents only a small portion (45%) of the overall inundated areas. Neglecting main linear infrastructures results in a significantly larger inundated region (i.e. 14 km^2 instead of 8 km^2 for Current and Infrastructures configuration), as the outflowing volume is not confined by man-made embankments, nor drained by the land-reclamation channel network (dark grey area in Fig. 4). Concerning Current and Infrastructures configuration, the barraging effects of transport infrastructures and the draining operated by artificial channels on the inundation dynamics are evident in Fig. 4 (black area); as a result, the computed water depths become higher in the central portion of the study area and the flooding moves northern towards the city centre.

These significant differences are even clearer if we consider the FAI values reported in Table 1. In particular, what is shown in Fig. 4 for one particular levee-breaching scenario (i.e. effects of infrastructures on current topography) is quantified by the values on the third row in Table 1 for the compound of four considered breaching locations. FAI values indicate that differences between the two terrain configurations in terms of significantly flooded areas relative to *h*, *v* or *i* vary approximately from 40% to 50%. Moreover, the FAI values resulting from the comparison between Current and Current and Infrastructures (third row in Table 1) correspond almost exactly to the FAI values obtained from the Past *vs.* Past and Infrastructures (fourth row in Table 1) or Past *vs.* Current and Infrastructures (fifth row in Table 1). This outcome highlights the overwhelming importance of considering or neglecting main linear discontinuities relative to anthropogenic land-subsidence observed in the study area. In conclusion, our analysis clearly shows that anthropogenic land-subsidence may have a role in altering inundation extent (or more precisely, the extent of significantly

inundated area), but its effects are marginal if compared with the impact of linear infrastructures in area surrounding the city of Ravenna.

Does this conclusion hold also for the spatial distribution of relevant hydraulic indices (i.e. *h*, *i*, and *v*)? To draw a firm conclusion on the role of anthropogenic land-subsidence and infrastructures, we further analysed all the flooding scenarios by assessing the changes in the spatial distribution of *h*, *v* and *i*. Referring in turn to one of the four breaching events, we compared pairs of terrain configurations by looking at spatial distribution of the difference of computed *h* (or *v*, or *i*) values, for all 5m cells, included in a reference area. This area is defined as the merger of all areas significantly inundated in terms of *h* (or *v*, or *i*) at least in one of the four configurations (i.e. Current, Past, Current and Infrastructures, Past and Infrastructures). For instance, if we consider Breach no. 1 - see Fig. 2(a) and the water depth *h* as hydraulic index, the reference area is the merger of the four areas that are significantly flooded in terms of *h* (water depths higher than 50 cm) for the four terrain configurations considered in the analysis.

Differences between flooding scenarios for two terrain configurations are evaluated in terms of empirical exceedance probability (or 1-*F*, if *F* is the empirical cumulative distribution function) of the absolute difference of computed water depths $|\Delta h|$ (or velocities, $|\Delta v|$, or intensities, $|\Delta i|$) over the reference area (i.e. merger of the four significantly flooded areas) discretized at 5m resolution. As a basis for all comparisons, we adopted Current and Infrastructures, which is the terrain configuration closer to reality (i.e., current topography with a detailed representation of all major linear infrastructures). All other terrain configurations (i.e., Past and Infrastructures, Current and Past*)* are therefore compared with Current and Infrastructures in terms of exceedance probability of $|\Delta h|$, $|\Delta v|$, and $|\Delta i|$, constructed by grouping together results obtained for all the four simulated levee-breaching scenarios. All other comparisons (e.g. Past vs. Past and Infrastructures, Past vs Current, Past and Infrastructures vs Current) are neglected because they do not provide any additional insight to the analysis.

Figure 5 presents the empirical exceedance probabilities for the three different hydraulic indices on three separate panels. Black lines refer to the comparison between Current and Infrastructures and Past and Infrastructures terrain configurations, which differ by means of anthropogenic ground-lowering only, while blue and red lines (Current and Infrastructures *vs.* Current and Current and Infrastructures *vs.* Past, respectively) highlight the influence of major linear infrastructures by comparing two terrain configurations that differ at least in terms of representation of main linear infrastructures. Grey areas in all panels highlight significant values of $|\Delta h|$ and $|\Delta v|$, that is differences within grey areas are higher than the typical uncertainty in variables modelled by TELEMAC-2D: $|\Delta h| = 0.2$ m, and $|\Delta v| = 0.2$ m s^{-1} (see Néelz and Pender 2013, Lim 2011, Dimitriadis *et al.* 2016); we calculated the uncertainty associated with simulated *i* (i.e. $|\Delta i|=0.08$ m^2 s^{-1}) by taking into account the propagation of uncertainties in *h* and *v*. Therefore, the larger the portion of the curves inside the grey areas, the lower the similarity between two flooding scenarios in terms of spatial distribution of either *h*, *v*, or *i*.

Results in Fig. 5 are in accordance with the previous findings: black lines show limited differences and small portions of the lines within the grey areas for h and v, whereas intensity i shows a slightly larger portion of the curve within the grey area (i.e. significant differences) due to the non-linear dependence on h and v.

Table 2 reports values of empirical exceedance probability for significant absolute differences (i.e. empirical probability associated with $|\Delta h| > 0.2$ m, $|\Delta v| > 0.2$ m s^{-1}, and $|\Delta i| > 0.08$ m^2 s^{-1}). These values can be interpreted also as the fractions of inundated areas in which differences between flooding scenarios on different terrain configurations in terms of computed water depth, velocity and current intensity are significant. Figure 5 and Table 2 support our findings in terms of extent of flooded areas (i.e. values reported in Table 1) and further highlight the limited influence of land-subsidence on flood hazard alteration, as the effects in terms of spatial alteration of hydraulic indices due to subsidence only are limited relative to the impact of linear infrastructures. The similarity between red and blue lines is evident in all panels of Fig. 5. These lines show the importance of main linear infrastructures, pointing out that differences between current configuration with and without linear infrastructures (red lines) are practically the same that one may obtain from the comparison between current topography with infrastructures and past topography without them (blue lines). It is, also, worth noting that portions of red and blue lines falling within grey areas in Fig. 5 are always significantly larger than the corresponding portion of black lines. This result is also evident from the three columns in Table 2.

Finally, by looking at Fig. 5 and Table 2, it is also evident that the alteration in terms of water depth and velocity (i.e. $|\Delta h|$ and $|\Delta v|$) associated with the presence of linear infrastructures is limited in all considered cases. The presence of infrastructures mostly affects the spatial distribution of flood intensity ($i = h \cdot v$), for which significant differences can be found in approx. 48% of flooded areas. In other terms, despite the alterations of computed water depth and velocity are significant only for small portions of the inundated areas (i.e. 14-20%), the product of the two is more sensitive to the terrain configuration and shows significant alterations over larger portions of inundated areas.

5.4 Sensitivity of results on Manning's roughness coefficient

Our study outcomes build on the results of TELEMAC-2D simulations that use an un-calibrated set of Manning's roughness coefficients. In order to assess the generality and robustness of the results of our study we performed a sensitivity analysis of the study outcomes on the Manning's coefficient focusing for simplicity on one breaching location only - i.e. location no. 2 in Fig. 2(a). We re-run all simulations relative to all four scenarios twice, by applying to the entire study area two different configurations of Manning coefficients for agricultural land-use and urban and industrial areas (see e.g. Werner *et al.* 2005 and Chow 1959 for agricultural areas and Liang *et al.* 2007 and Bellos and Tsakiris 2015 for build-up areas). In particular, we considered a low-roughness condition ("Min n" in Fig. 6) that adopts $n = 0.10$ m$^{-1/3}$s for urban and industrial areas and 0.022 m$^{-1/3}$s for agricultural areas, and a high-roughness condition adopting a uniform $n = 0.2$ m$^{-1/3}$s over the entire

study area ("Max n" in Fig. 6). Min n and Max n aim at assessing the sensitivity of our outcomes to reasonable alternative values of *n*, relative to our reference condition: n = 0.2 $m^{-1/3}s$ for urban and industrial areas and 0.035 $m^{-1/3}s$ for agricultural areas ("Adopted n" in Fig. 6).

Figure 6 illustrates the difference we obtained in terms of $|\Delta h|$ values for the same three comparisons illustrated in Figure 5: Current and Infrastructures vs. Past and Infrastructures (black, top panel); Current and Infrastructures vs. Current (blue, middle panel); Current and Infrastructures vs. Past (red, bottom panel). Figure 6 adopts the same colours used in Fig. 5. In particular, bold lines in Figure 7 illustrate the exceedance probability of $|\Delta h|$ values for breach location 2 and adopted configuration of Manning roughness coefficient, whereas dashed and dotted lines illustrate the results we obtained by adopting the maximum and minimum roughness conditions, respectively. Similar results were obtained in terms of $|\Delta v|$ and $|\Delta i|$, and are not illustrated here for the sake of brevity.

All panels of Fig. 6 clearly indicate that the sensitivity of our results to Manning's roughness coefficient is rather limited when Current and Infrastructures is compared against all other scenarios. Even though we are referring to rather different parameterizations of TELEMAC-2D, the results of our sensitivity analysis confirm that what drives most of the changes in inundation intensity are linear infrastructures (middle and lower panel of Fig. 6), whereas anthropogenic land-subsidence has a very limited impact (upper panel of Fig. 6). Also, the limited extent of shaded areas between "Min n" and "Max n" configurations in all panels of Fig. 6 are a clear indication of the limited sensitivity of the main outcomes of our study on Manning's *n*; the larger differences that are visible in the right and lower ends of the curves (see in particular the top panel) are an artefact of the log-scale used for *y* axes.

6 CONCLUSIONS

We studied the effects of anthropogenic land-subsidence on riverine flood hazard, comparing it with the impact on flooding intensity of artificial channels and road or railway embankments. We considered the area close to the city of Ravenna (Italy), as it is the most prominent example of human-accelerated land-subsidence in Italy. Due to an intense extraction of underground water and natural gas, the study area underwent an extremely significant ground-lowering during the last century, with a cumulative drop higher than 1.5 m in a century in the historical centre of the city, horizontal gradients above 0.3 m km^{-1}, and lowering rates larger than 110 mm $year^{-1}$, when the natural rate is estimated in a few mm $year^{-1}$ (see Gambolati *et al.* 1991, Carminati and Martinelli 2002, Teatini *et al.* 2005).

We simulated different levee breaches along the Montone-Ronco river system and then assessed and compared the computed flooding intensity of the adjacent flood-prone area resulting from four alternative terrain configurations, that is the current topography with and without main artificial road and railways embankments and channels, and the reconstructed topography for year 1897, with and without main artificial embankments and channels. Inundation scenarios were compared to each other in terms of computed flooded

areas and spatial distribution of computed water depth (h) and velocity (v) and current intensity ($i = h \cdot v$) of the current.

The main outcome of our analysis is that large and rapid differential land-subsidence observed in the study area may have produced modifications of riverine flood hazard, yet these alterations do not seem to be significant. In fact, the most significant and evident changes in flood hazard occurring in the study area seem to be associated with the construction of main linear hydraulic and transport infrastructures (i.e. man-made land-reclamation and irrigation channels and road or railway embankments). These discontinuities introduce macroscopic alterations of the inundated areas and spatial distribution of hydrodynamic variables that are certainly more important than alterations resulting from man-induced, or man–accelerated, land-subsidence.

Consequently, under the main assumptions of our study, which focuses solely on topographical modifications induced by land-subsidence while neglecting changes in any other potential natural and anthropogenic diver of flood-hazard dynamics (e.g. land-use and land-cover changes, expansion of built-up areas, etc.), we can conclude for the study area that anthropogenic land-subsidence may be seen as potential driver of riverine flood hazard (and consequently flood-risk) changes, but the construction of artificial canals and road embankments has a definitely stronger control on flooding potential.

Although the limited relevance of anthropogenic land-subsidence relative to alteration in inundation intensity, it is still necessary to consider its effect in terms of ground-lowering gradients, which alter the safety level of rivers embankments, and hence flood hazard. This aspect deserves to be investigated in detail in future analyses.

Additionally, our analysis further shows that a correct assessment and mapping of flood hazard and risk that rely on hydrodynamic inundation modelling cannot dispense with an accurate representation of major topographic discontinuities, such as artificial irrigation and land-reclamation channel systems and road and railway embankments (i.e. resolution should be finer than 5 m). More in general, the results highlight the importance of accurately identifying specific topographic data that have to be considered in the modelling exercise (Dottori *et al.* 2013, Domeneghetti 2014), which should represent the best compromise to balance model complexity, efficiency, and reliability.

ACKNOWLEDGEMENTS

The present work was developed within the framework of the Panta Rhei Research Initiative of the International Association of Hydrological Sciences (IAHS). The Emilia-Romagna Region, Regional Agency for Civil Protection, and regional river basins authorities are kindly acknowledged for providing the datasets used in the study.

FUNDING

Funding was partly provided by the University of Bologna, the SYSTEM-RISK Marie-Skłodowska-Curie European Training Network (EU grant 676027).

REFERENCES

AdB-Reno, AdB-RR, and AdB-Marecchia-Conca, 2016. *Piano di gestione del rischio alluvioni.*

AdB-RR, 2011. *Piano Stralcio per il Rischio Idrogeologico – Variante al Titolo II "Assetto della rete idrografica".*

Barkau, R.L., 1997. *UNET One dimensional Unsteady Flow through a full network of open channels user's manual*. Davis, CA: US Army Corps of Engineering, Hydrologic Engineering Center.

Bellos, V., and Tsakiris, G., 2015. Comparing Various Methods of Building Representation for 2D Flood Modelling In Built-Up Areas. *Water Resources Management* 29(2), 379–397.

Bitelli, G., Bonsignore, F., and Unguendoli, M., 2000. Levelling and GPS networks to monitor ground subsidence in the Southern Po Valley. *Journal of Geodynamics*, 30, 355–369.

Bouwer, L.M., Bubeck, P., and Aerts, J.C.J.H., 2010. Changes in future flood risk due to climate and development in a Dutch polder area. *Global Environmental Change - Human and Policy Dimensions*, 20, 463–471.

Brath, A., and Di Baldassarre, G., 2006. Modelli matematici per l'analisi della sicurezza idraulica del territorio. *L'Acqua*, 6, 39–48.

Brown, S., and Nicholls, R.J., 2015. Subsidence and human influences in mega deltas: The case of the Ganges–Brahmaputra–Meghna. *Science of the Total Environment*, 527–528, 362–374.

Carisi, F., Domeneghetti, A., Castellarin, A., 2015. Simplified graphical tools for assessing flood-risk change over large flood-prone areas. *PIAHS*, 92, 1–7.

Carminati, E., and Martinelli, G., 2002. Subsidence rates in the Po Plain, northern Italy: the relative impact of natural and anthropogenic causation. *Engineering Geology*, 66, 241–255.

Castellarin, A., Di Baldassarre, G., and Brath, A., 2011. Floodplain management strategies for flood attenuation in the river Po. *River Research and Applications*, 27, 1037-1047.

Chow, V. T., 1959. *Open Channel Hydraulics*, McGraw-Hill, New York.

Ciullo, A., Viglione, A., Castellarin, A., Crisci, M., and Di Baldassarre, G., 2016. Socio-hydrological modelling of flood risk dynamics: Comparing the resilience of green and technological systems. *Hydrological Sciences Journal*, *62*(6), 880–891.

Daito, K. and Galloway, D.L., 2015. Preface: Prevention and mitigation of natural and anthoropogenic hazards due to land subsidence. *PIAHS*, 372, 555–557.

Di Baldassarre, G., Castellarin, A., and Brath, A., 2009a. Analysis of the effects of levee heightening on flood propagation: example of the river Po, Italy. *Hydrological Sciences Journal*, 54, 1007–1017.

Di Baldassarre, G., Castellarin, A., Montanari, A., and Brath, A., 2009b. Probability weighted hazard maps for comparing different flood risk management strategies: a case study. *Natural Hazards*, 50, 479– 496.

Di Baldassarre, G., Kooy, M., Kemerink, J.S., and Brandimarte, L., 2013. Towards understanding the dynamic behaviour of floodplains as human-water systems. *Hydrology and Earth System Sciences*, 17(8), 3235–3244.

Dimitriadis, P., Tegos, A., Oikonomou, A., Pagana, V., Koukouvinos, A., Mamassis, N., Koutsoyiannis, D., and Efsrìtratiadis, A., 2016. Comparative evaluation of 1D and quasi-2D hydraulic models based on benchmarks and real-world applications for uncertainty assessment in flood mapping. *Journal of Hydrology*, 534, 478-492.

Domeneghetti, A., Vorogushyn, S., Castellarin, A., Merz, B., and Brath, A., 2013. Probabilistic flood hazard mapping: Effects of uncertain boundary conditions. *Hydrology and Earth System Sciences*, 17, 3127–3140.

Domeneghetti, A., 2014. Effects of minor drainage networks on flood hazard evaluation. *PIAHS*, 364, 192–197.

Domeneghetti A., Carisi, F., Castellarin, A., and Brath, A., 2015. Evolution of flood risk over large areas: Quantitative assessment for the Po river. *Journal of Hydrology*, 527, 809–823.

Dottori, F., Di Baldassarre, G., and Todini, E., 2013. Detailed data is welcome, but with a pinch of salt: Accuracy, precision, and uncertainty in flood inundation modeling. *Water Resources Research*, 49, 6079–6085.

European Environment Agency (EEA), 2016. *CORINE Land Cover 2012 (CLC2012), 100 m*. Copenhagen, Denmark.

Falter, D., Vorogushyn, S., Lhomme, J., Apel, H., Gouldby, B., and Merz, B., 2013. Hydraulic model evaluation for large-scale flood risk assessments. *Hydrological Processes*, 27(9), 1331–1340.

Fernandes, E.H., Dyer, K.R., and Niencheski, L.F.H., 2001. Calibration and validationof the TELEMAC-2D model to the Patos Lagoon (Brazil). *Journal of Coastal Research*, 34, 470-488.

Gaeta, M.G., Samaras, G., Federico, I., Archetti, R., Maicu, F., and Lorenzetti, G., 2016. A coupled wave-3-D hydrodynamics model of the Taranto Sea (Italy): a multiple-nesting approach, *Natural Hazards and Earth System Sciences*, 16, 2071-2083.

Galland, J.C., Goutal, N., and Hervouet, J.M., 1991. TELEMAC: a new numerical model for solving shallow water equations. *Advances in Water Resources*, 14, 38–148.

Gambolati, G., Ricceri, G., Bertoni, W., Brighenti, G., and Vuillermin, E., 1991. Mathematical simulation of the subsidence of Ravenna. *Water Resources Research*, 27, 2899–2918.

Gotoh, H., Takezawa, M., Maeno, Y., Oshiki, H., Nagashima, S., Nishimura, Y., and Ohta, M., 2009. Development and restoration of the urban rivers: examples from old downtown Tokyo, Japan. *WIT Transactions on Ecology and the Environment - River Basin Management V*, 124(1), 69-80.

Govi, M., and Turitto, O., 2000. *Casistica storica sui processi d'iterazione delle correnti di piena del Po con arginature e con elementi morfotopografici del territorio adiacente (Historical documentations about*

the processes of dam breaks in the River Po, in Italian). Milan, Italy: Istituto Lombardo Accademia di Scienza e Lettere.

Green, C., Viavattene, C., and Thompson, P., 2011. *Guidance for assessing flood losses - CONHAZ Report*, London: Middlesex University, CONHAZ Consortium.

Guha-Sapir, D., Below, R., and Hoyois, Ph. *EM-DAT: The CRED/OFDA International Disaster Database – www.emdat.be*. Université Catholique de Louvain, Brussels, Belgium.

HEC (Hydrologic Engineering Center), 2010. *HEC–RAS river Analysis System – User's Manual, Version 4.1*, Davis, CA: US Army Corps of Engineering, Hydrologic Engineering Center.

Hailemariam, F.M., Brandimarte, L., and Dottori, F., 2013. Investigating the influence of minor hydraulic structures on modelling flood events in lowland areas. *Hydrological Processes*, 28(4), 1742-1755.

Hervouet, J.M., and Van Haren, L., 1996. Recent advances in numerical methods for fluid flows. *In*: M.G. Anderson, D.E. Walling, and P.D. Bates eds. *Floodplain Processes*. Chichester, UK: John Wiley & Sons Ltd., 183–214.

Horritt, M.S., Di Baldassarre, G., Bates, P.D., and Brath, A., 2007. Comparing the performance of 2-D finite element and finite volume models of floodplain inundation using airborne SAR imagery. *Hydrological Processes*, 21, 2745–2759.

Howladar, M.F., and Hasan, K., 2014. A study on the development of subsidence due to the extraction of 1203 slice with its associated factors around Barapukuria underground coal mining industrial area, Dinajpur, Bangladesh. *Environmental Earth Sciences*, 72, 3699–3713.

Kreibich, H., Piroth, K., Seifert, I., Maiwald, H., Kunert, U., Schwarz, J., Merz, B., and Thieken. A.H., 2009. Is flow velocity a significant parameter in flood damage modelling?. *Natural Hazards and Earth System Sciences*, 9(5), 1679–1692.

Koutsoyiannis, D., 2013. Hydrology and change. *Hydrological Sciences Journal*, 58 (6), 1177–1197.

Liang, D., Falconer, R. A., and Lin, B., 2007. Coupling surface and subsurface flows in a depth averaged flood wave model. *Journal of Hydrology*, 337, 147–158.

Lim, N.J., 2011. *Performance and uncertainty estimation of 1- and 2-dimensional flood models*. Thesis (BSc), Gävle University College, Sweden.

Marfai, M. A., and King, L., 2008. Tidal inundation mapping under enhanced land subsidence in Semarang, Central Java Indonesia. *Natural Hazards*, 44(1), 93–109.

Merz, B., Kreibich, H., and Lall, U., 2013. Multi-variate flood damage assessment: A tree-based data-mining approach. *Natural Hazards and Earth System Sciences*, 13(1), 53-64.

Meyer, V., Becker, N., Markantonis, V., Schwarze, R., Van Den Bergh, J.C.J.M., Bouwer, L.M., and Viavattene, C., 2013. Review article: assessing the costs of natural hazards- state of the art and knowledge gaps. *Natural Hazards and Earth System Sciences*, 13, 1351–1373.

Molinari, D., Menoni, S., Aronica, G.T., Ballio, F., Berni, N.,Montanari, A., Young, G., Savenije, H.H.G., Hughes, D., Wagener, T., Ren, L.L., Koutsoyiannis, D., Cudennec, C., Toth, E., Grimaldi, S., Blöschl, G., Sivapalan, M., Beven, K., Gupta, H., Hipsey, M., Schaefli, B., Arheimer, B., Boegh, E., Schymanski,

S.J., Di Baldassarre, G., Yu, B., Hubert, P., Huang, Y., Schumann, A., Post, D., Srinivasan, V., Harman, C., Thompson, S., Rogger, M., Viglione, A., McMillan, H., Characklis, G., Pang, Z., and Belyaev, V., 2013. ‘‘Panta Rhei—Everything Flows’’: change in hydrology and society—the IAHS scientific decade 2013–2022. *Hydrological Sciences Journal*, 58(6), 1256-1275.

Néelz, S., and Pender, G., 2013. *Delivering benefits through evidence – Benchmarking the latest generation of 2D hydraulic modelling packages*. Bristol, UK: Environment Agency, Department for Environment, Food and Rural Affairs.

Orlandini, S., Moretti, G., and Albertson, J., 2015. Evidence of an emerging levee failure mechanism causing disastrous floods in Italy. *Water Resources Research*, 51(10), 7995–8011.

Ortega-Guerrero, A., Rudolph, D.L., and Cherry, J.A., 1999. Analysis of long-term land subsidence near Mexico City: Field investigations and predictive modeling. *Water Resources Research*, 35(11), 3327-3341.

Phien-wej, N., Giao, P.H., and Nutalaya, P., 2006. Land subsidence in Bangkok, Thailand. *Engineering Geology*, 82(4), 187–201.

Potok, A. J., 1991. A Study of the Relationship between Subsidence and Flooding. In *Proceedings of the Fourth International Symposium on Land Subsidence*, 200, 389-396, Houston, Texas, USA.

Rodolfo, K. S. and Siringan, F. P., 2006. Global sea-level rise is recognised, but flooding from anthropogenic land subsidence is ignored around northern Manila Bay, Philippines. *Disasters*, 30(1), 118-139.

Teatini, P., Ferronato, M., Gambolati, G., Bertoni, W., and Gonella, M., 2005. A century of land subsidence in Ravenna, Italy. *Environmental Geology*, 47(6), 831–846.

Schmidt, C.W., 2015. Delta subsidence – An imminent threat to coastal populations. *Environmental Health Perspectives*, 123, 204–209.

Schumann, G., Bates, P.D., Horritt, M.S., Matgen, P., and Pappenberger, F., 2009. Progress in integration of remote sensing-derived flood extent and stage data and hydraulic models. *Reviews of Geophysics*, 47(3), 1-21.

Sivapalan, M., Savenjie, H.G., and Blöschl, G., 2012. Socio-hydrology: A new science of people and water. *Hydrological Processes*, 26, 1270–1276.

Vorogushyn, S., 2008. Analysis of flood hazard under consideration of dike breaches. Thesis (PhD), Universität Potsdam, Germany.

Werner, M.G.F., Hunter, N.M., Bates, P.D., 2005. Identifiability of distributed floodplain roughness values in flood extent estimation, *Journal of Hydrology*, 314, 139-157.

Yin J., Yu, D., Yin, Z., Wang, J., and Xu, S., 2013. Modelling the combined impacts of sea-level rise and land subsidence on storm tides induced flooding of the Huangpu river in Shanghai, China. *Climatic Change*, 119, 919–932.

Zanchettini, D., Traverso, P., and Tomasino, M., 2008. Po river discharge: a preliminary analysis of a 200-year time series. *Climatic Change*, 88, 411–433.

TABLES

Table 1 FAI values in terms of *h*, *v* and *i* resulting from the comparison of different configurations. Each value is the average of the values obtained, for the same pair of compared terrain configurations, in all the four considered levee-breaching scenarios.

	FAI (*h*)	FAI (*v*)	FAI (*i*)
Current *vs.* Past (Effect of subsidence neglecting linear infrastructures)	0.88	0.81	0.83
Current and Infrastructures *vs.* Past and Infrastructures (Effect of subsidence considering linear infrastructures)	0.93	0.77	0.87
Current *vs.* Current and Infrastructures (Effect of linear infrastructures on current topography)	0.50	0.47	0.58
Past *vs.* Past and Infrastructures (Effect of linear infrastructures on past topography)	0.51	0.49	0.58
Past *vs.* Current and Infrastructures (Effect of both subsidence and linear infrastructures)	0.50	0.49	0.58

Table 2 Fraction of inundated areas that are associated with significant differences between pairs of terrain configurations in terms of computed maximum water depth $|\Delta h|$, velocity $|\Delta v|$, and intensity $|\Delta i|$.

	Current and Infrastructures *vs.* Past and Infrastructures (Impact of subsidence)	Current and Infrastructures *vs.* Current (Impact of infrastructures)	Current and Infrastructures *vs.* Past (Impact of subsidence and infrastructures)
$\|\Delta h\|$	0.01	0.20	0.19
$\|\Delta v\|$	0.02	0.14	0.14
$\|\Delta i\|$	0.08	0.48	0.48

FIGURES

Figure 1 Study area: location of the Ravenna municipality and urban area (a and b) and Digital Elevation Model of the cumulative land-subsidence between 1897 and 2002 (c); see Teatini *et al.* 2005)

Figure 2 Study area: current topography (5m-resolution DEM), major infrastructures considered in the study (with relative embankments' height and channels' depth) and locations of the hypothesized levee breaches (a); non-structured computational mesh used for all 2D simulations in TELEMAC-2D (b).

Figure 3 Example of different inundation patterns associated with the same levee breaching (breach no. 2, indicated in red) and two different terrain configurations: *Curr (*Current topography), and Past (reconstruction of the pre anthropogenic land-subsidence topography). Main linear infrastructures are neglected.

Figure 4 Example of different inundation patterns associated with the same levee breaching (breach no. 2, indicated in red) and two different terrain configurations: *Curr (*Current topography), and *Curr_Infr (*Current and Infrastructures*)*, that is current topography with main linear infrastructures (i.e. roads and railways embankments, land-reclamation channels).

Figure 5 Empirical exceedance probability of $|\Delta h|$, $|\Delta v|$, and $|\Delta i|$ (y axes in log-scale) between pairs of levee-breaching scenarios on different terrain configurations; grey areas denote the range of significant absolute differences.

Figure 6 Sensitivity analysis of the study results to Manning's roughness coefficient: empirical exceedance probability of $|\Delta h|$ (y axes in log-scale) between pairs of levee-breaching scenarios on different terrain configurations referring to different roughness coefficients ("Adopted n" = 0.2 $m^{-1/3}s$ for urban and industrial areas and 0.035 $m^{-1/3}s$ for agricultural area; "Min n" = 0.1 $m^{-1/3}s$ for urban and industrial areas and 0.02 $m^{-1/3}s$ for agricultural area; "Max n" = 0.2 $m^{-1/3}s$ for the entire study area); grey areas denote the range of significant absolute differences.

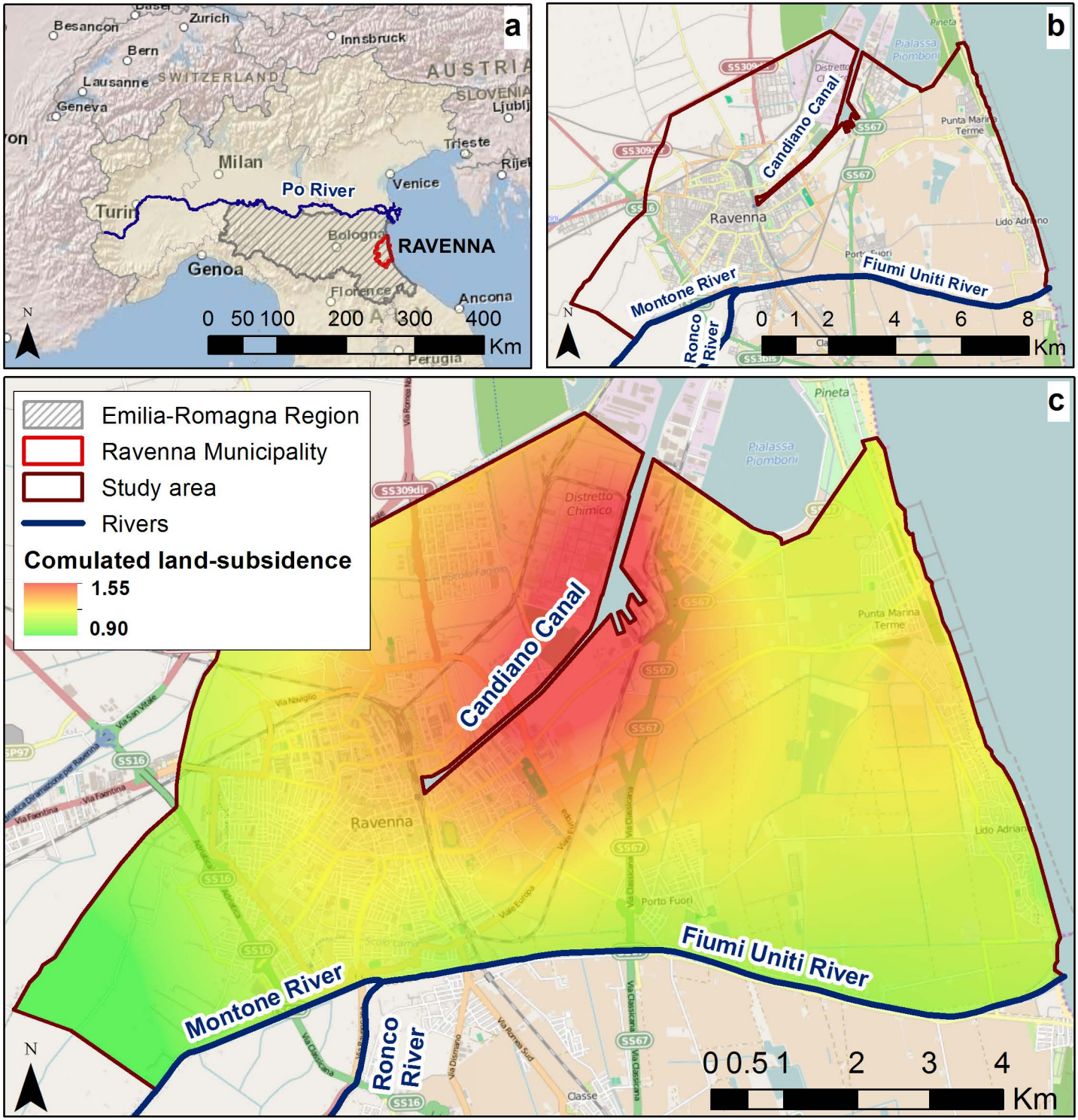
a
Besancon
Zurich
Innsbruck
Bern
SWITZERLAND
AUSTRIA
Lausanne
Geneva
SLOVENIA
Ljubl
Trieste
Milan
Venice
Po River
Turin
Bologna
RAVENNA
Genoa
Florence
Ancona
Perugia
N
0 50 100 200 300 400
Km
b
Pineta
Pialassa Piomboni
Candiano Canal
Punta Marina Terme
Ravenna
Lido Adriano
Montone River
Fiumi Uniti River
Ronco River
0 1 2 4 6 8
Km
c
Emilia-Romagna Region
Ravenna Municipality
Study area
Rivers
Comulated land-subsidence
1.55
0.90
Distretto Chimico
Candiano Canal
Punta Marina Terme
Ravenna
Porto Fuori
Lido Adriano
Fiumi Uniti River
Montone River
Ronco River
Classe
N
0 0.5 1 2 3 4
Km

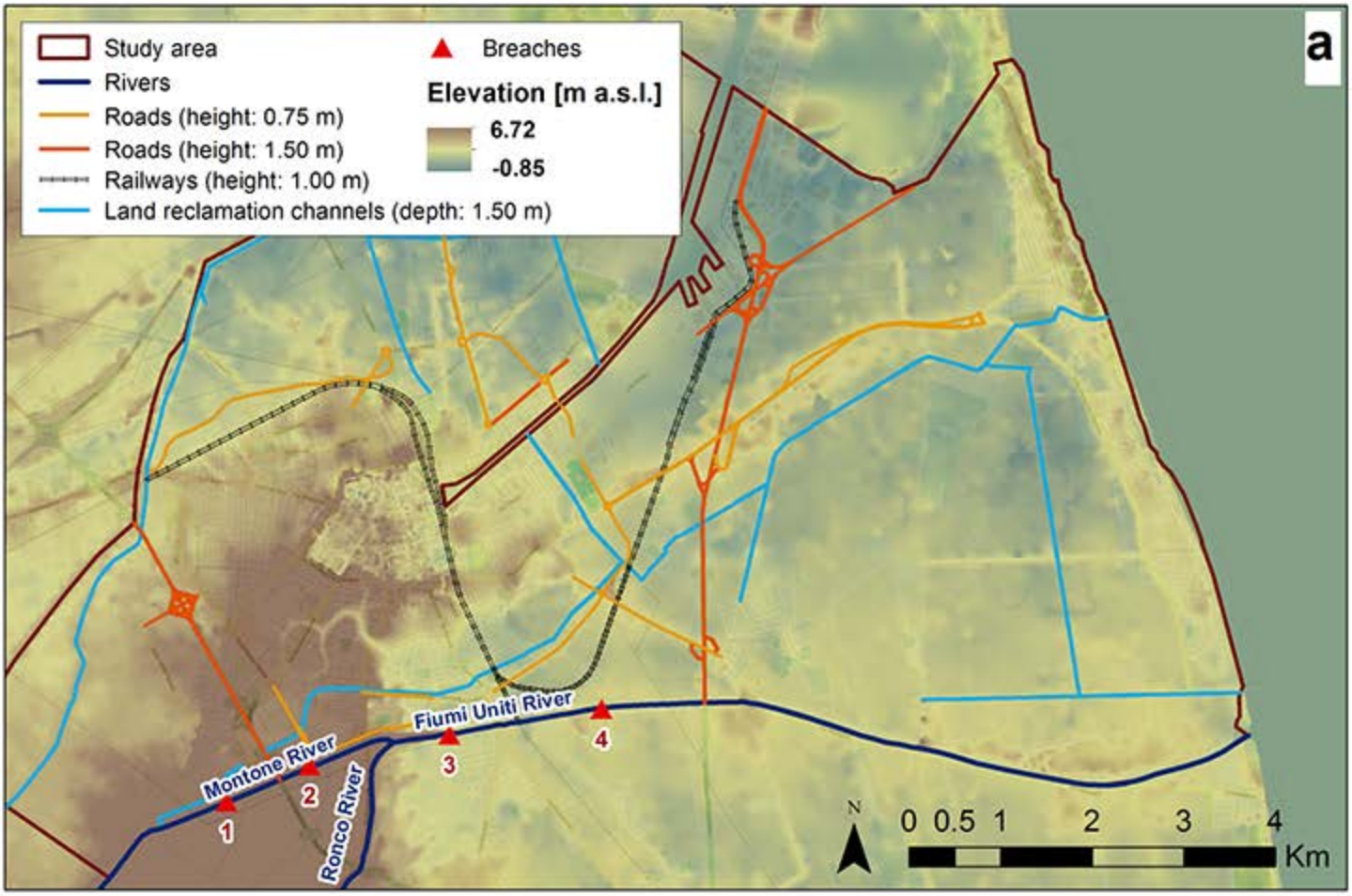
Study area
Rivers
Roads (height: 0.75 m)
Roads (height: 1.50 m)
Railways (height: 1.00 m)
Land reclamation channels (depth: 1.50 m)
Breaches
Elevation [m a.s.l.]
6.72
-0.85
a
Montone River
Fiumi Uniti River
Ronco River
1
2
3
4
N
0 0.5 1 2 3 4
Km

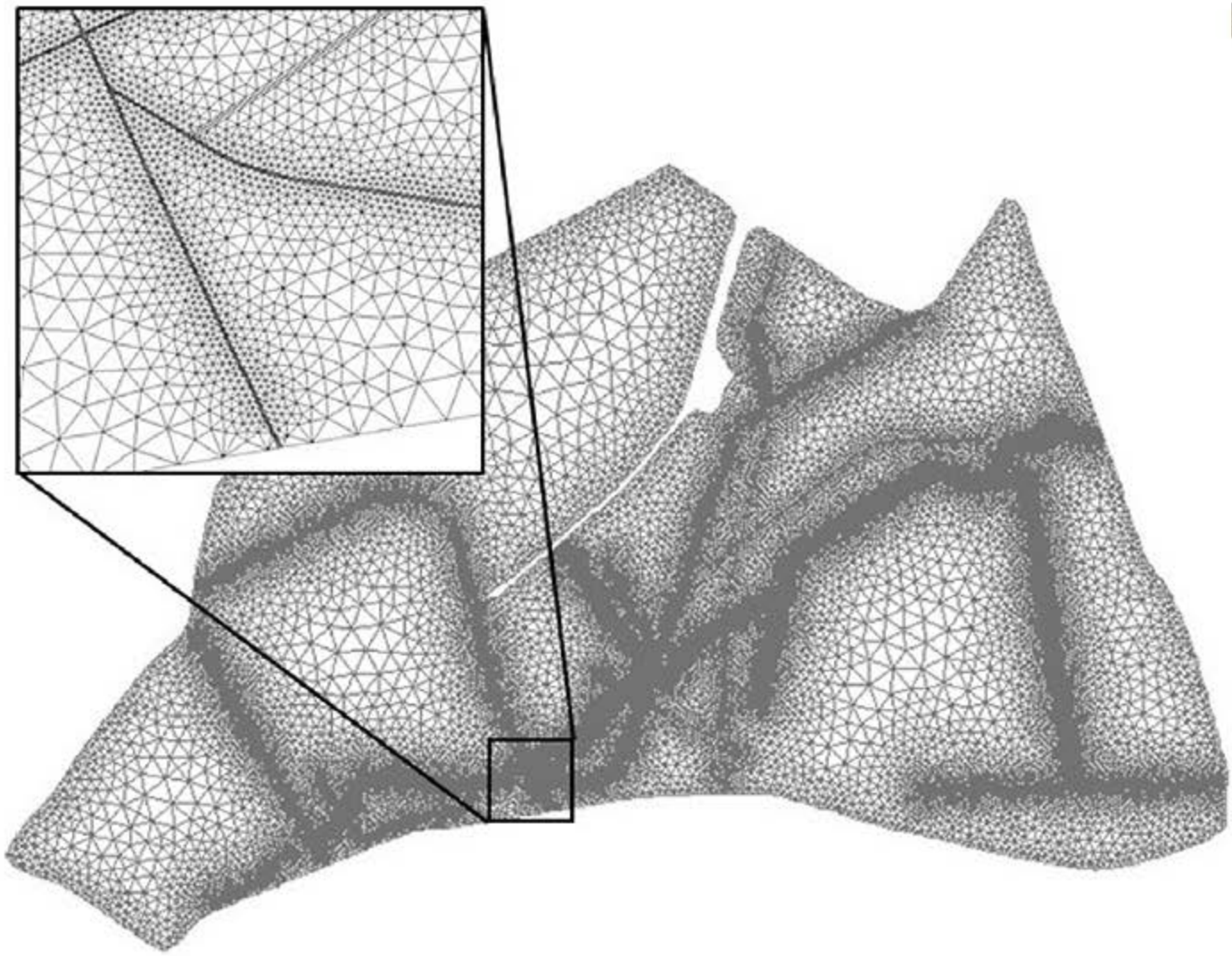
b

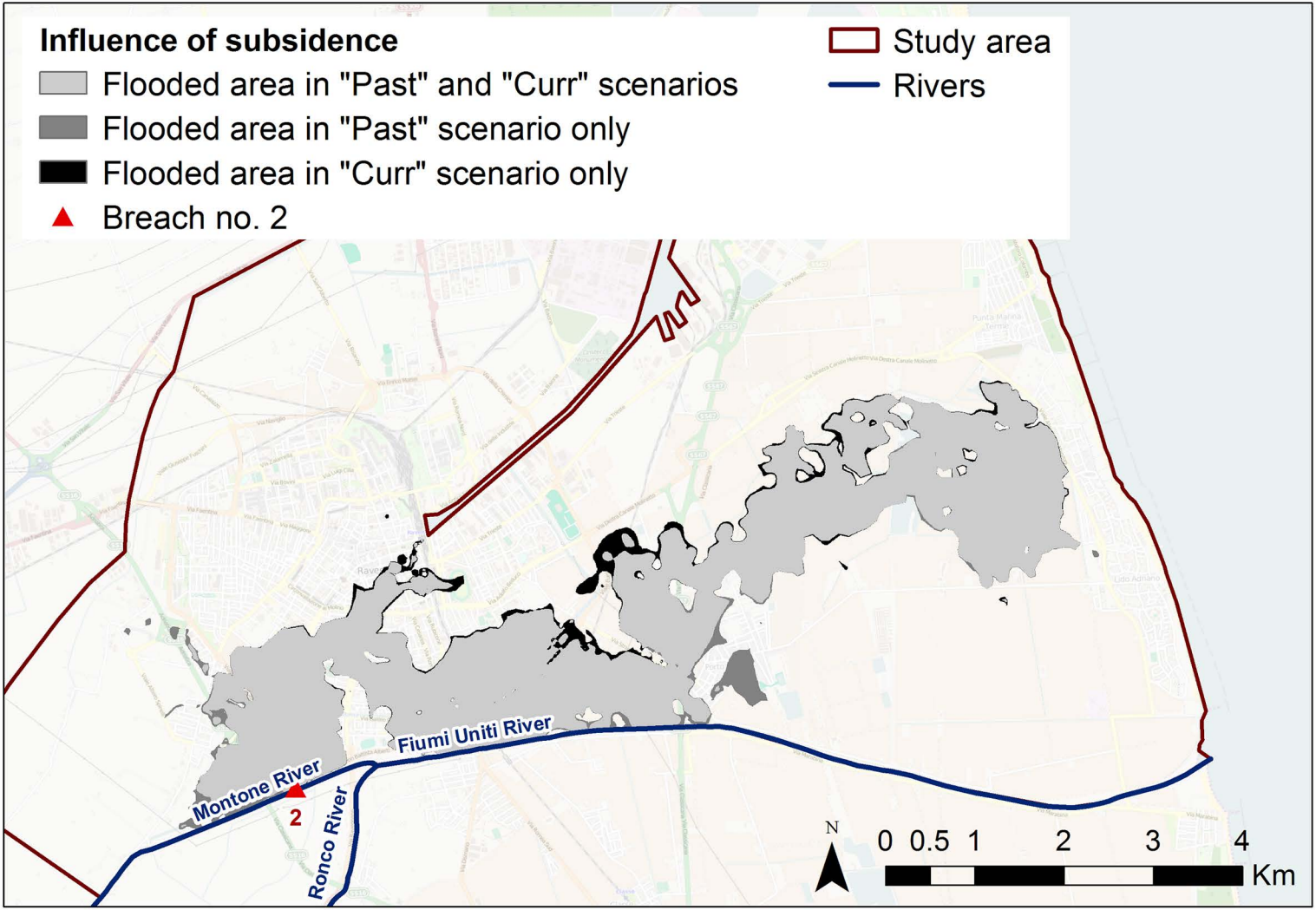
Influence of subsidence
Flooded area in "Past" and "Curr" scenarios
Flooded area in "Past" scenario only
Flooded area in "Curr" scenario only
Breach no. 2
Study area
Rivers
Montone River
Fiumi Uniti River
Ronco River
2
N
0 0.5 1 2 3 4
Km

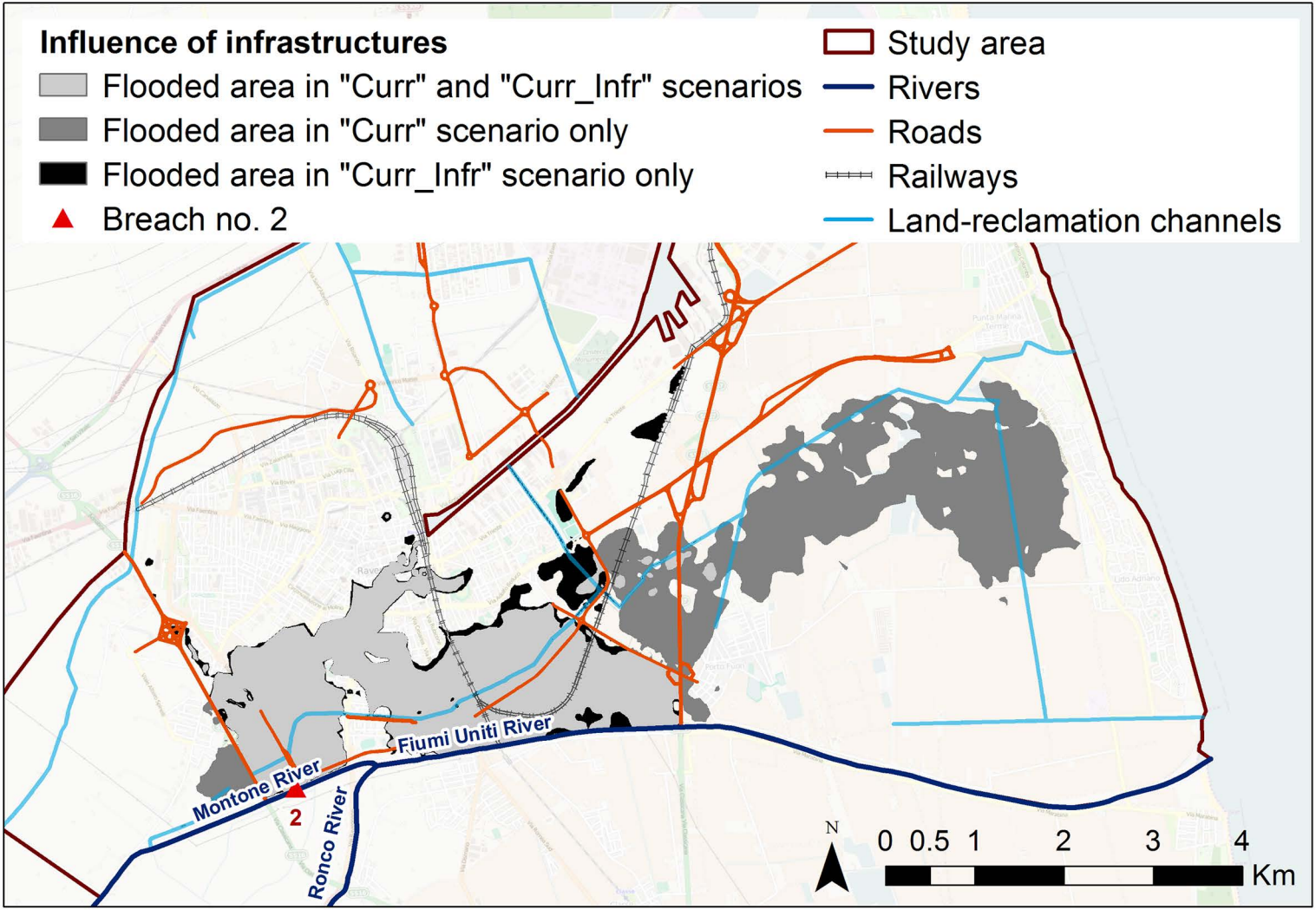
Influence of infrastructures
Flooded area in "Curr" and "Curr_Infr" scenarios
Flooded area in "Curr" scenario only
Flooded area in "Curr_Infr" scenario only
Breach no. 2
Study area
Rivers
Roads
Railways
Land-reclamation channels
Fiumi Uniti River
Montone River
Ronco River
2
N
0 0.5 1 2 3 4
Km

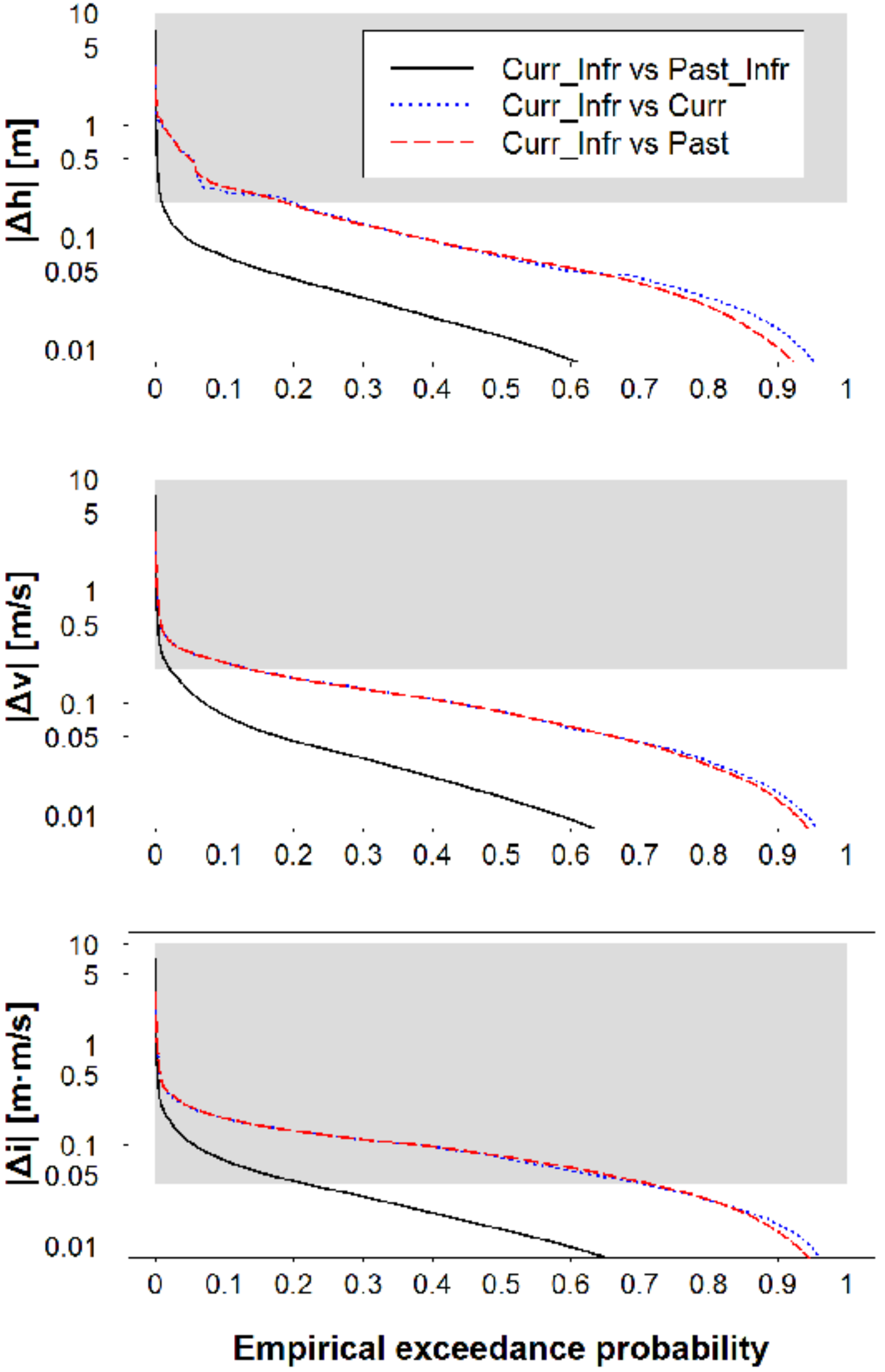
Curr_Infr vs Past_Infr
Curr_Infr vs Curr
Curr_Infr vs Past
|Δh| [m]
|Δv| [m/s]
|Δi| [m·m/s]
10
5
1
0.5
0.1
0.05
0.01
0
0.1
0.2
0.3
0.4
0.5
0.6
0.7
0.8
0.9
1
Empirical exceedance probability

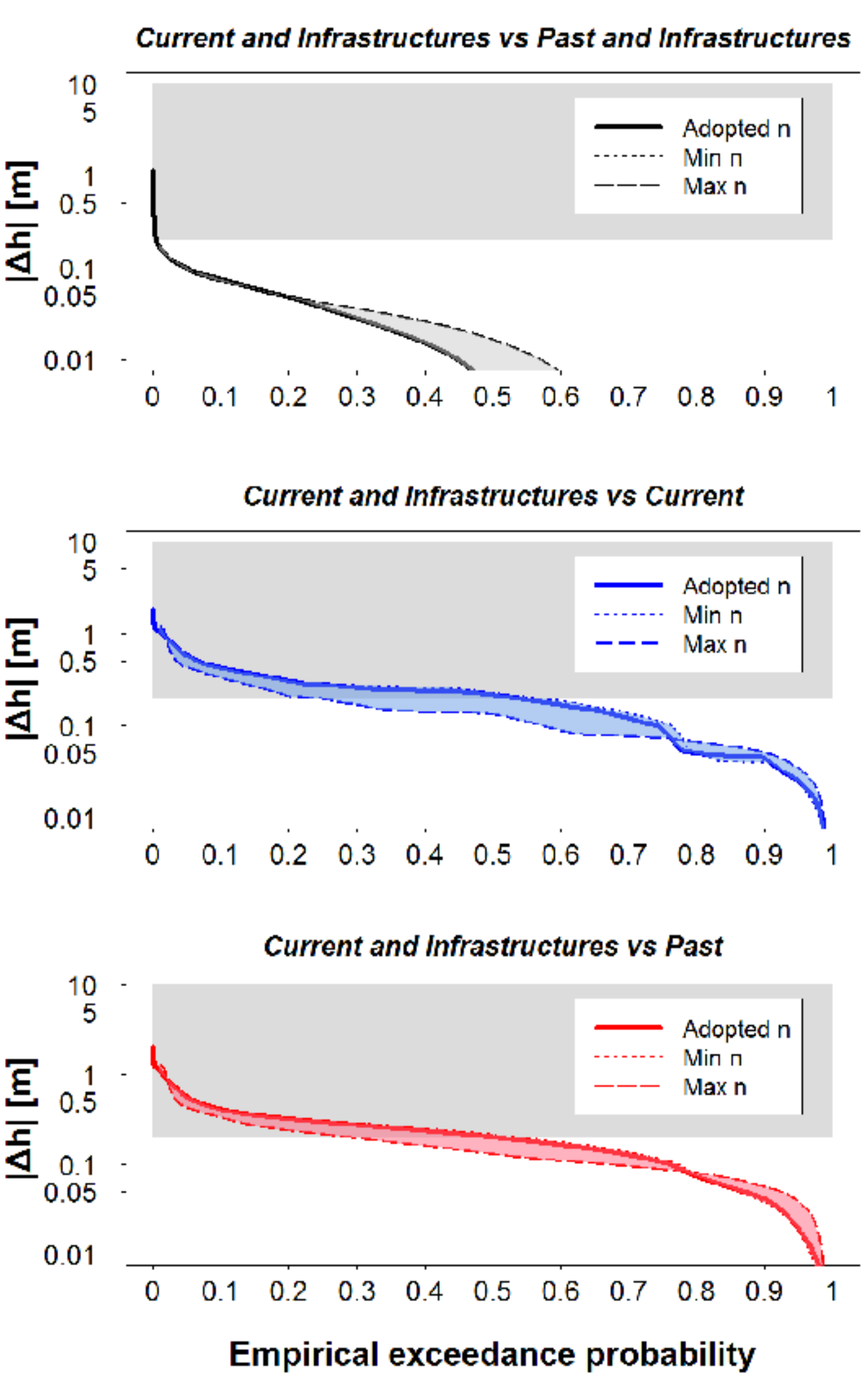
Current and Infrastructures vs Past and Infrastructures
Adopted n
Min n
Max n
|Δh| [m]
10
5
1
0.5
0.1
0.05
0.01
0
0.1
0.2
0.3
0.4
0.5
0.6
0.7
0.8
0.9
1
Current and Infrastructures vs Current
Adopted n
Min n
Max n
|Δh| [m]
Current and Infrastructures vs Past
Adopted n
Min n
Max n
|Δh| [m]
Empirical exceedance probability